Appl Magn Reson (2026) 57:11
https://doi.org/10.1007/s00723-026-01829-9

Applied
Magnetic Resonance

RESEARCH

Comparative Spectroscopic Investigation of Amyloid Beta Peptides Spin-Labeled with MTSL and PROF

Johannes Mause[1] · Lisa Ebo[1] · Miriam Hülsmann[2] · Annalisa Pierro[1] · Adelheid Godt[2] · Malte Drescher[1,3] · Mykhailo Azarkh[1]

Received: 19 November 2025 / Revised: 26 January 2026 / Accepted: 5 February 2026

Abstract

The ability of electron paramagnetic resonance (EPR) spectroscopy to handle heterogeneous samples is particularly valuable to study structure and dynamics of intrinsically disordered proteins/peptides (IDPs). Such proteins lack a well-defined secondary structure. Site-directed spin-labeling (SDSL), which is the introduction of paramagnetic labels, must ensure that the properties of IDPs remain intact. In this work, amyloid beta (Aβ) peptides spin labeled with the non-canonical amino acid PROF and with MTSL bound to cysteine are investigated and compared. Focusing on the structural integrity and aggregation behavior, it is shown that PROF is a suitable spin label for Aβ. Spin labeling with both PROF and MTSL leads to similar characteristic structural details of Aβ peptides, i.e., random coil and β-sheets, as well as similar rotational mobility in solution. The use of the non-canonical amino acid PROF for spin labeling of IDPs can be superior in respect to linker stability, particularly in EPR studies under physiological conditions, and when naturally occurring cysteines are essential for the protein function.

1 Introduction

Intrinsically disordered proteins (IDPs) are a class of proteins that are under physiological conditions conformationally highly flexible and, therefore, lack a well-defined structure. They play crucial roles in biological processes, such as signal transduction and regulation [1, 2]. The highly dynamic structural flexibility of

✉ Mykhailo Azarkh
mykhailo.azarkh@uni-konstanz.de

[1] Department of Chemistry and Konstanz Research School Chemical Biology, University of Konstanz, Universitätsstr. 10, 78457 Constance, Germany

[2] Faculty of Chemistry and Center for Molecular Materials (CM2), Bielefeld University, Universitätsstraße 25, 33615 Bielefeld, Germany

[3] Present Address: RPTU University Kaiserslautern-Landau, 67663 Kaiserslautern, Germany

Published online: 19 February 2026

IDPs enables diverse interactions with other proteins and has been linked to several neurodegenerative diseases, including Alzheimer's disease (AD) [3]. A prominent example of an IDP associated with AD pathogenesis is amyloid beta (Aβ), which is generated by proteolytic cleavage of the amyloid precursor protein, primarily via the sequential actions of β- and γ-secretases [4, 5]. Dysregulation of Aβ production or impaired clearance mechanisms can lead to its pathological accumulation, resulting in amyloid plaque formation [6–8]—a hallmark of AD pathology [8–11]. AD is the most common neurodegenerative disease, accounting for 60–70% of all dementia cases [12]. Worldwide, over 55 million people are affected, with approximately 10 million new cases each year, underscoring its significant impact [13, 14].

The lack of one well-defined structure makes IDPs challenging to study with methods such as X-ray crystallography or cryo-EM which rely on a single conformation [15–18]. For such cases, electron paramagnetic resonance spectroscopy combined with site-directed spin labeling (SDSL) is a powerful tool. It is widely used for investigating structure and dynamics of proteins on the molecular level [15–19]. Small nitroxide spin labels are of particular advantage for investigating the dynamics of proteins [20, 21], as they minimize structural perturbation upon labeling [22, 23]. Nitroxides are stable across a wide range of conditions [24] and their anisotropy, g-tensor and hyperfine coupling provide detailed insights into local dynamics during EPR spectroscopical experiments [23, 25, 26]. While a single spin label, attached to a protein or a peptide, reports on its local environment and dynamics [27–29], two labels provide structural information. Utilizing pulsed EPR spectroscopy [30, 31], the distance distribution between two paramagnetic centers can be determined [30, 32–37]. Importantly, the more rigidly the spin label is connected to the protein, the more the distance distribution is determined by the structural properties of the spin-labeled molecule.

A well-established spin labeling approach is the attachment of a nitroxide radical to a cysteine being either native to the protein/peptide or introduced by site-directed mutagenesis or solid-phase synthesis. The most commonly used nitroxide is 1-oxyl-2,2,5,5-tetramethyl-2,5-dihydro-1H-pyrrol [38]. It is most often attached to the thiol group of a cysteine via disulfide bond formation using the labeling agent 1-oxyl-2,2,5,5-tetramethyl-2,5-dihydro-1H-pyrrol-3-yl)methyl methanethiosulfonate, which gives the MTSL-labeled cysteine, C(MTSL) shown in Fig. 1a. A notable drawback of using the thiol group of cysteine for labeling of aggregation-prone proteins is the frequent occurrence of incomplete labeling [39]. In such cases, solvent-accessible, unlabeled cysteines can form disulfide bonds [40], potentially compromising the protein's structural integrity [41]. Investigations of MTSL-labeled proteins within cells, where reducing conditions prevail, face the additional challenge of the reductive cleavage of the disulfide bond and, therefore, the detachment of the nitroxide [42, 43]. In addition, the cellular environment reduces nitroxides, rendering them silent for detection via EPR [44, 45].

A spin labeling approach that utilizes non-canonical amino acids in general offers several advantages for site-specific labeling compared to methods based on cysteines [46–48]. Non-canonical amino acids with azide or alkyne groups offer the possibility of a site-specific attachment of nitroxides via the copper-catalyzed cycloaddition reaction between an azide and an alkyne. This attachment of the nitroxide can take

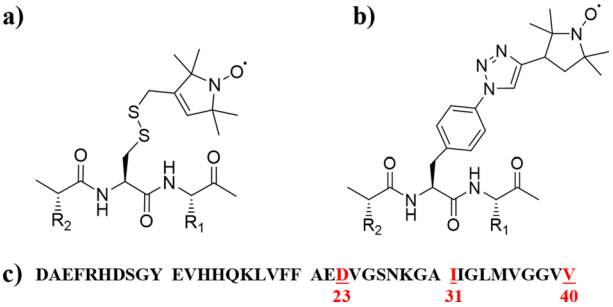

Fig. 1 Chemical structure of **a** MTSL-labeled cysteine and **b** the non-canonical amino acid PROF incorporated in a peptide backbone and **c** amino acid sequence of $A\beta^{wt}$ with the labeling sites 23, 31 and 40 (red)

place either before or after incorporation of the non-canonical amino acid into the protein sequence. In such cases, site-directed mutagenesis is required only at the position, where the non-canonical amino acid should be incorporated, whereas cysteine-based labeling involves the introduction of a cysteine at the desired site and, if present, the substitution of native cysteines to avoid off-target labeling [49–51]. When incorporating non-canonical amino acids, it is not necessary to replace native cysteines, which may be crucial for the peptide's function [52, 53]. In addition, the triazole linker formed during the copper-catalyzed click reaction is resistant to the reducing cellular environment, in contrast to the relatively labile disulfide bond of an MTSL-labeled cysteine.

In this work, we focus on the nitroxide bearing amino acid proxyl-labeled phenylalanine (PROF) (Fig. 1b). This amino acid was recently shown to be introducible by site-directed mutagenesis followed by post-translational modification via copper-catalyzed click reaction [30, 54]. It provides distance distributions comparable to those determined with the C(MTSL). It is also possible to use PROF in solid-phase synthesis, at least for short peptides. Here, we address the question whether PROF is suitable for spin labeling of IDPs, which are known to be very sensitive to structural changes, and compare PROF with C(MTSL). We focus on structural characteristics and rotational mobility of Aβ equipped with PROF and C(MTSL).

2 Results and Discussion

The peptide sequence of wild-type Aβ, $A\beta^{wt}$, is shown in Fig. 1c. The underlined red letters indicate the positions (23, 31, and 40), where the naturally occurring amino acids were replaced by either PROF or C(MTSL). The positions for spin labeling have been selected such that CD and EPR spectroscopical data could be obtained for cases, where spin labeling disturbs the protein structure as well as for cases, where it does not disturb the structure. All three positions lie outside the metal-binding region, which is comprised of the first 16 residues at the N-terminus. Residues 31

and 40 are located at the C-terminus. According to literature reports, these residues can become a part of the fiber core (PDB codes: 2mvx, 2m4j) [55, 56]. Residue D23 is known to be crucial for the aggregation of Aβ [57]. Spin labeling of this site has been used as a negative control. In the following, the three spin-labeled Aβ variants are denoted as $A\beta^{PROFn}$ and $A\beta^{C(MTSL)n}$, depending on the type of nitroxide-labeled amino acid [PROF or C(MTSL)] and its position *n* in the peptide sequence.

First, the case is considered where Aβ was labeled at position 40, which is the C-terminus. Replacing the valine at this site is expected to have a minor to no impact on the structure and properties of the peptide. In the case of $A\beta^{C(MTSL)40}$, the carboxyl group of the C-terminus was converted into a carboxamide group, because cysteine as the C-terminal amino acid is prone to undergo a side reaction during the peptide synthesis (private communication, Biosyntan GmbH, Berlin).

Circular dichroism (CD) measurements were performed to elucidate the secondary structure, while EPR measurements were performed to analyze the rotational mobility of the nitroxide under aggregating and non-aggregating conditions. Details of EPR spectral simulations and individual spectral components are given in the Supporting information.

Figure 2 shows the results of CD and EPR spectroscopical measurements of $A\beta^{PROF40}$ and $A\beta^{C(MTSL)40}$ at pH 11.5 and pH 6.5. Under non-aggregating conditions (pH 11.5), the CD spectrum of $A\beta^{wt}$ exhibits the shape typical of a molecule with a random-coil conformation, with a minimum at 200 nm (Fig. 2a). The spectrum of $A\beta^{PROF40}$ exhibits a similar shape, but that of $A\beta^{C(MTSL)40}$ looks quite different from a pronounced minimum at 220 nm, which is typical for the presence of β-sheets [58]. Please be reminded of the different C-terminus: carboxylic acid in case of PROF and carboxamide in case of C(MTSL).

The EPR spectra of both spin-labeled Aβ variants look the same and their shapes are typical for fast tumbling nitroxides in solution (Fig. 2b). The quantitative analysis of the EPR spectra via simulation reveals that the spectra can be described with rotational correlation times τ_r of 0.16 ns for $A\beta^{C(MTSL)40}$ and 0.26 ns for $A\beta^{PROF40}$ (Table 1). These τ_r values are typically found for Aβ with a mobile spin label and freely tumbling peptide [20, 59]. The slightly larger τ_r value of $A\beta^{PROF40}$ as compared to $A\beta^{C(MTSL)40}$ indicates a lower conformational flexibility of the sidechain of PROF as compared to the side chain of C(MTSL). This can be understood considering the difference in the number of single bonds—5 single bonds in the case of C(MTSL) and 4 single bonds in the case of PROF (Fig. 1).

In addition, TEM images were taken of dried $A\beta^{wt}$, $A\beta^{PROF40}$ and $A\beta^{C(MTSL)40}$ showing that the overall morphology of Aβ remained unchanged upon labeling (see Supporting Information).

Under aggregating conditions (pH 6.5), the CD spectrum of $A\beta^{wt}$ displays a minimum at 220 nm, indicative of a β-sheet structure (Fig. 2c). Both spin-labeled Aβ variants, $A\beta^{PROF40}$ and $A\beta^{C(MTSL)40}$, exhibit comparable spectral profiles, indicating that their secondary structure does not differ from that of $A\beta^{wt}$. The reduced intensities of the signals of the CD spectra at pH 6.5 as compared to those at pH 11.5 can be attributed to large aggregates which, if larger than the wavelength, scatter light in random direction thus reducing the amount of light reaching the detector [58]. The EPR spectra of the spin-labeled Aβ variants at pH 6.5 are given in Fig. 2d. The

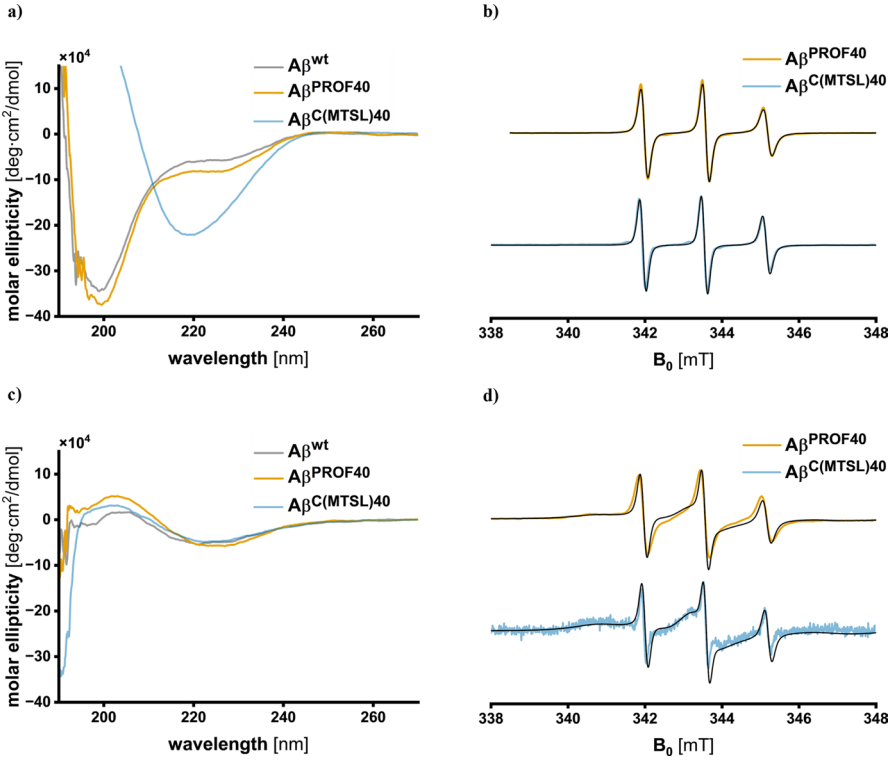

Fig. 2 CD spectra of $A\beta^{wt}$ (grey), $A\beta^{PROF40}$ (orange) and $A\beta^{C(MTSL)40}$ (blue) under **a** non-aggregating (pH 11.5) and **c** aggregating conditions (pH 6.5); EPR spectra of $A\beta^{PROF40}$ (orange) and $A\beta.^{C(MTSL)40}$ (blue) under **b** non-aggregating and **d** aggregating conditions and spectral simulations (black)

Table 1 Parameters used for spectral simulations of the EPR spectra of Aβ variants recorded at pH 11.5 and pH 6.5

pH 11.5	$A\beta^{C(MTSL)23}$		$A\beta^{PROF23}$		$A\beta^{C(MTSL)31}$		$A\beta^{PROF31}$		$A\beta^{C(MTSL)40}$		$A\beta^{PROF40}$	
Fraction [%]	12	88	17	83	100		100		100		100	
τ_r [ns]	0.4	4	0.4	4	0.4		0.4		0.16		0.26	
Heisenberg exchange interaction [MHz]	0	5	0	5	0		0		0		0	
pH 6.5												
Fraction [%]	0	100	1	99	16	84	8	92	6	94	12	88
τ_r [ns]	0.4	5	0.4	5	0.4	5	0.4	5	0.16	5	0.26	5
Heisenberg exchange interaction [MHz]	0	10	0	10	0	10	0	10	0	10	0	10

spectra are similar with well-pronounced three peaks. These peaks are broader as compared to those in the EPR spectra at pH 11.5 (Fig. 2b). Such broadening can arise from a reduction in the rotational mobility of the spin label and from dipolar interaction between close-by electron spins, both being potential results of peptide aggregation. In addition to the three peaks, the spectra show a broad peak at around 341 mT. This indicates the presence of several spectral components and, consequently, several states of Aβ in solution. Indeed, spectral simulations reveal for both variants the superposition of two spectral components, a fast and a slow component. The fast component with a rotation correlation time of 0.16 ns for $A\beta^{C(MTSL)40}$ and 0.26 ns for $A\beta^{PROF40}$ describes species with high rotational mobility. These data are identical with the data found for the spin-labeled Aβ variants under non-aggregating conditions (pH 11.5) and, therefore, are taken as an indication that monomeric species are present at pH 6.5. The slow component, causing the additional broad peak at around 341 mT, has a rotational correlation time of 5 ns for both spin-labeled Aβ variants. This slow rotation can be explained by the presence of Aβ aggregates, which effectively decreases the rotational mobility of the nitroxide. The simulation of the experimental data can be improved by adding a line broadening referring to Heisenberg spin exchange (10 MHz), which accounts to the interaction between nitroxides due to their close proximity when spin-labeled molecules aggregate (Table 1). The percentage of the slow component is 88% for $A\beta^{PROF40}$ and 94% for $A\beta^{C(MTSL)40}$, indicating the presence of a slightly higher amount of aggregates in case of $A\beta^{C(MTSL)40}$ (Table 1). However, the simulated spectra deviate slightly from the experimental ones. Therefore, the difference in the percentage of the slow component for $A\beta^{PROF40}$ and $A\beta^{C(MTSL)40}$ has to be viewed with care. In any case, the EPR spectra of both spin-labeled Aβ variants is dominated by the slow component.

As in the case of non-aggregating conditions, TEM images show the same overall morphology for all three peptides $A\beta^{wt}$, $A\beta^{PROF40}$ and $A\beta^{C(MTSL)40}$ when dried (see Supporting Information).

Next, the case is considered, where the spin label was incorporated at position 31, replacing the isoleucine, which is close to the middle of the peptide. As this site is neither hydrophobic nor located within the metal-binding region, the modification at this site is assumed not to affect the structure or properties of Aβ.

At non-aggregating conditions (pH 11.5), the CD spectra of $A\beta^{wt}$, $A\beta^{PROF31}$, and $A\beta^{C(MTSL)31}$ exhibit a similar shape with a pronounced minimum at 200 nm, typical for molecules with a random-coil structure (Fig. 3a). The EPR spectra of both spin-labeled Aβ variants are typical for fast rotating nitroxides (Fig. 3b). Quantitative analysis via spectral simulations reveals that the spectra can be described with only one spectral component, with a rotational correlation time τ_r of 0.4 ns for both peptides (Table 1). This value is larger than determined for $A\beta^{PROF40}$ and $A\beta^{C(MTSL)40}$. Obviously, the correlation time arises from the coupled motion of the peptide chain and the nitroxide. This agrees with the finding that the closer the nitroxide is placed to the middle of Aβ, the larger is the influence of the peptide chain itself to the dynamics of the nitroxide [60].

At aggregating conditions (pH 6.5), the CD spectra show similar features for $A\beta^{wt}$, $A\beta^{PROF31}$, and $A\beta^{C(MTSL)31}$ (Fig. 3c). The CD spectra display a minimum around 220 nm, characteristic for β-sheet structure, and an overall low signal

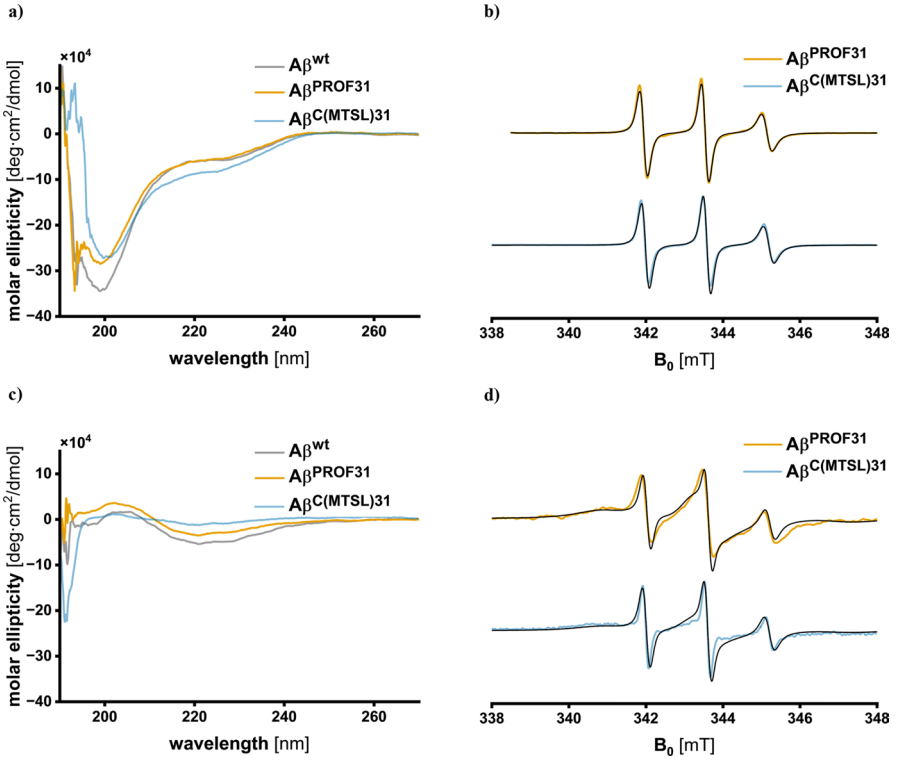

Fig. 3 CD spectra of $A\beta^{wt}$ (grey), $A\beta^{PROF31}$ (orange) and $A\beta^{C(MTSL)31}$ (blue) under **a** non-aggregating (pH 11.5) and **c** aggregating conditions (pH 6.5); EPR spectra of $A\beta^{PROF31}$ (orange) and $A\beta.^{C(MTSL)31}$ under **b** non-aggregating and **d** aggregating conditions and spectral simulations (black)

intensity caused by larger aggregates. The EPR spectra of $A\beta^{PROF31}$ and $A\beta^{C(MTSL)31}$ are similar in their spectral shape. They show three lines with significant broadening (Fig. 3d). Quantitative analysis via spectral simulation reveals two spectral components for both spectra. In both cases, the fast spectral component has a rotational correlation time τ_r of 0.4 ns which indicates the presence of Aβ in its monomeric form (Fig. 3b). The slow spectral component has a correlation time τ_r of 5 ns, a Heisenberg exchange interaction of 10 MHz and is attributed to Aβ aggregates. The fractions of the slow component are 92% for $A\beta^{PROF31}$ and 84% for $A\beta^{C(MTSL)31}$, which indicate that the slow spectral component is dominant and Aβ is mainly present in aggregated form (Table 1).

Aβ contains amino acids, whose modification can significantly impair its structure, function and aggregation. Such an amino acid is the aspartic acid at position 23. To investigate how spin-labeling at such a critical position affects the CD and EPR spectra, PROF and C(MTSL) were incorporated at position 23, replacing the aspartic acid.

Under non-aggregating conditions (pH 11.5), the CD spectra of $A\beta^{PROF23}$ and $A\beta^{C(MTSL)23}$ differ significantly from that of the $A\beta^{wt}$ (Fig. 4a). While the CD

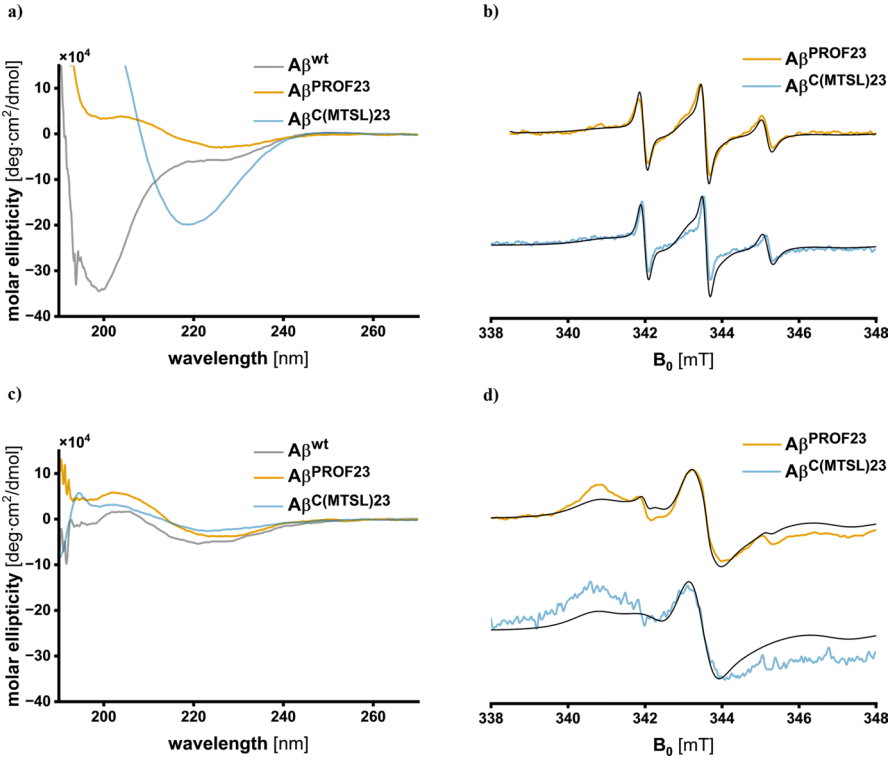

Fig. 4 CD spectra of $A\beta^{wt}$ (grey), $A\beta^{PROF23}$ (orange) and $A\beta^{C(MTSL)23}$ (blue) under **a** non-aggregating (pH 11.5) and **c** aggregating conditions (pH 6.5); EPR spectra of $A\beta^{PROF23}$ (orange) and $A\beta.^{C(MTSL)23}$ under **b** non-aggregating and **d** aggregating conditions and spectral simulations (black)

spectrum of $A\beta^{wt}$ exhibits the typical shape of a random-coil spectrum with a minimum at 200 nm, the spectra of the spin-labeled Aβ variants show a minimum at 220 nm. This minimum is characteristic for β-sheets. It is more pronounced in the CD spectrum of $A\beta^{C(MTSL)23}$ than in that of $A\beta^{PROF23}$. The EPR spectra of $A\beta^{PROF23}$ and $A\beta^{C(MTSL)23}$ display three significantly broadened lines (Fig. 4b). Quantitative analysis allowed for identification of two spectral components, which are necessary to describe the experimental EPR spectra. For both spin-labeled Aβ variants, the fast component has a correlation time τ_r of 0.4 ns and the slow component a correlation time τ_r of 4 ns with a Heisenberg exchange interaction of 5 MHz. The correlation time of the fast component fits to that of monomeric Aβ. The slow component is assigned to aggregates. The fractions of the slow component are 83% for $A\beta^{PROF23}$ and 88% for $A\beta^{C(MTSL)23}$ (Table 1). Obviously, even under non-aggregating conditions aggregates prevail.

Under aggregating conditions (pH 6.5), the CD spectra of the $A\beta^{wt}$, $A\beta^{PROF23}$ and $A\beta^{C(MTSL)23}$ are very similar to each other (Fig. 4c). They feature a minimum at 220 nm and overall low signal intensity, indicating the presence of β-sheets and

the presence of aggregates which reduce the amount of light reaching the detector. The EPR spectra of $A\beta^{PROF23}$ and $A\beta^{C(MTSL)23}$ are similar in shape (Fig. 4d); however, they differ significantly from the spectra of the other spin-labeled Aβ variants. Notably, the spectral lines are extremely broad, a characteristic of slowly rotating nitroxides, corresponding to τ_r values on the order of a few nanoseconds. Spectral simulations provide further quantitative insight. Neither of the two spectra can be satisfactorily simulated using one fast and one slow component. The EPR spectrum of $A\beta^{C(MTSL)23}$ does not show any presence of the fast spectral component. An approximation of the experimental spectrum using only a slow component with a correlation time τ_r of 5 ns turned out to be insufficient. The spectral shape of the EPR spectrum of $A\beta^{PROF23}$ can be approximated by the superposition of a slow component with $\tau_r = 5$ ns with an exchange interaction of 10 MHz and a very small contribution from a fast component with $\tau_r = 0.4$ ns. The slow component is dominating with a fraction of 99% (Table 1). Whereas the fast component exhibits the same τ_r value of 0.4 ns as in the simulations for the pH 11.5 spectrum, the τ_r value of the slow component has increased slightly from 4 nm to 5 ns. It is suggested that additional contributions and/or spectral components influence the spectral shape, as a consequence of high structural heterogeneity of Aβ. However, they are not resolved in the spectrum to a degree that allows identification.

Summarizing, under non-aggregating conditions (pH 11.5), $A\beta^{PROF40}$, $A\beta^{PROF31}$, and $A\beta^{C(MTSL)31}$ adopt a structure similar to that of $A\beta^{wt}$. In contrast, $A\beta^{C(MTSL)40}$, $A\beta^{PROF23}$, and $A\beta^{C(MTSL)23}$ adopt a β-sheet structure. We suspect that the difference between $A\beta^{PROF40}$ and $A\beta^{C(MTSL)40}$ is caused by the different C-termini: a carboxyl group in case of $A\beta^{PROF40}$ and a carboxamide group in case of $A\beta^{C(MTSL)40}$. That such a little change has such an impact on the secondary structure of Aβ shows how sensitive an IDP can be. That $A\beta^{PROF23}$ and $A\beta^{C(MTSL)23}$, which both have a carboxyl group at the C-terminus, exhibit a β-sheet structure shows that the peptide structure is also determined through the position of labeling.

The EPR spectra of $A\beta^{PROF40}$, $A\beta^{C(MTSL)40}$, $A\beta^{PROF31}$ and $A\beta^{C(MTSL)31}$ under non-aggregating conditions can be well-described by a single fast component with a rotational correlation time τ_r between 0.2 and 0.4 ns. The rotation is slower for Aβ labeled at position 31 than for Aβ labeled at position 40. This is interpreted as a result of a coupled mobility of the peptide and the spin label. The nitroxide located at the C-terminus is more flexible compared to the nitroxide attached at the middle of the peptide.

The EPR spectra of $A\beta^{PROF23}$ and $A\beta^{C(MTSL)23}$ can only be described by a superposition of a fast and a slow component, indicating with CD data a partial aggregation even at pH 11.5. This highlights the unsuitability of position 23 for spin labeling.

Under aggregating conditions (pH 6.5), all investigated Aβ variants exhibit the same β-sheet secondary structure in the CD spectra as $A\beta^{wt}$. The EPR spectra of Aβ spin-labeled at position 31 or 40 show a feature at ~ 341 mT, which is characteristic for nitroxides with restricted rotational mobility. Spectral simulations describe these spectra as a superposition of a nitroxide not restricted in tumbling and a

slow-rotating, aggregated component, with the latter being dominant with a contribution of more than 80%.

3 Conclusions

The non-canonical amino acids PROF and C(MTSL) were examined as spin labels for investigating aggregation processes of Aβ, an important representative for an IDP. With the spectroscopic methods CD and EPR the secondary structure of the peptide and the rotational mobility of the spin label were determined. In addition, the EPR spectroscopical data revealed the degree of aggregation. With the combination of the two spectroscopic methods, positions at Aβ could be determined that are suitable for modification without compromising the secondary structure of this peptide. PROF proved to be as suitable as C(MTSL). This is of particular interest, because the non-canonical amino acid PROF offers increased linker stability in reducing environments, due to the absence of a disulfide bond, and selective labeling, if native cysteines are essential for protein function.

4 Methods

4.1 Synthesis of Spin-Labeled Aβ Variants

The amino acid PROF was synthesized as described by Stehle et al. [30] All peptides were synthesized by Biosynthan (Berlin, Germany). The Fmoc-protected PROF was incorporated into the Aβ peptide sequence at position 23, 31 or 40 via solid phase synthesis and the peptides were obtained with an HPLC purity of > 90%. C(MTSL) variants were obtained by solid phase synthesis introducing a cysteine at position 23, 31 or 40, followed by labeling with 1-oxyl-2,2,5,5-tetramethyl-2,5-dihydro-1H-pyrrol-3-yl)methyl methanethiosulfonate and were obtained with an HPLC purity of > 90%. The peptide sequences are displayed in Table 2.

Table 2 Peptide sequences of the spin-labeled Aβ variants

Aβ peptide	Peptide sequence
$A\beta^{wt}$	*H*-DAEFRHDSGY EVHHQKLVFF AEDVGSNKGA IIGLMVGGVV-*OH*
$A\beta^{C(MTSL)23}$	*H*-DAEFRHDSGY EVHHQKLVFF AE-**C(MTSL)**-VGSNKGA IIGLMVGGVV-*OH*
$A\beta^{C(MTSL)31}$	*H*-DAEFRHDSGY EVHHQKLVFF AEDVGSNKGA -**C(MTSL)**-IGLMVGGVV-*OH*
$A\beta^{C(MTSL)40}$	*H*-DAEFRHDSGY EVHHQKLVFF AEDVGSNKGA IIGLMVGGVV-**C(MTSL)**-NH_2
$A\beta^{PROF23}$	*H*-DAEFRHDSGY EVHHQKLVFF AE-**PROF**-VGSNKGA IIGLMVGGVV-*OH*
$A\beta^{PROF31}$	*H*-DAEFRHDSGY EVHHQKLVFF AEDVGSNKGA -**PROF**-IGLMVGGVV-*OH*
$A\beta^{PROF40}$	*H*-DAEFRHDSGY EVHHQKLVFF AEDVGSNKGA IIGLMVGGVV-**PROF**-*OH*

Highlinghting spin-labeled sites in bold increases the readability of the amino acid sequence, which is given in plain capitals

4.2 Sample Preparation for Non-aggregating Conditions

The lyophilized peptides were dissolved in a 10 mM NaOH solution containing 100 mM NaCl at pH 11.5 to reach a concentration of 1 mM and sonicated for 10 min. This solution was diluted with a 10 mM NaOH solution with pH 11.5 and glycerol-d_8 to obtain a sample containing 20 vol.% glycerol-d_8 and being 100 µM in Aβ. Glycerol-d_8 was added as a cosolvent, because it is planned to study the samples with double electron–electron resonance (DEER) spectroscopy as well.

4.3 Sample Preparation for Aggregating Conditions

The lyophilized peptides were dissolved in a 10 mM NaOH solution containing 100 mM NaCl with pH 11.5 to reach a concentration of 1 mM and sonicated for 10 min. This solution was diluted with a 10 mM phosphate buffer (69% NaH_2PO_4, 31% Na_2HPO_4) with pH 6.5 and glycerol-d_8 to obtain a sample containing 20 vol.% glycerol-d_8 and being 100 µM in Aβ. Glycerol-d_8 was added as a cosolvent, because it is planned to study the samples with double electron–electron resonance (DEER) spectroscopy as well.

4.4 Circular Dichroism Spectroscopy

For the CD measurements, 100 µL of the peptide solution were filled into a 0.5 mm demountable cuvette (QS High Precision Cell, Hellma Analytics). CD spectra were measured with a JASCO J-715 spectropolarimeter at 20 °C within the range of 180–280 nm. The raw data were baseline corrected and the background spectra subtracted.

4.5 EPR Spectroscopy

EPR measurements were performed on a BRUKER EMXnano X-band continuous wave EPR spectrometer. Samples were filled in HIRSCHMANN ringcaps® capillaries and closed with Chaseal tube sealing compound. All spectra were recorded at 20 °C with a modulation amplitude of 1 G, a modulation frequency of 100 kHz and a microwave power of 3.162 mW. Baseline correction and EPR simulations were performed on MATLAB R2022b with the Easyspin package [61].

Acknowledgements Financial support from the Young Scholar Fund of the University of Konstanz is highly acknowledged.

Author contributions Conceptualization: MD, MA, JM; Methodology: AG, MD, MA; Formal analysis and investigation: JM, LE, MH, AP; Writing—original draft preparation: JM, AG, MA; Writing—review and editing: all authors; Supervision: AG, MD, MA.

Funding Open Access funding enabled and organized by Projekt DEAL.

Data availability All the experimental data are available from the authors upon request.

Declarations

Conflict of interest The authors declare no competing interests.

References

1. A.K. Dunker, S.E. Bondos, F. Huang, C.J. Oldfield, Semin. Cell Dev. Biol. **37**, 44 (2015). https://doi.org/10.1016/j.semcdb.2014.09.025
2. P. Tompa, E. Schad, A. Tantos, L. Kalmar, Curr. Opin. Struct. Biol. **35**, 49 (2015). https://doi.org/10.1016/j.sbi.2015.08.009
3. V.N. Uversky, V. Davé, L.M. Iakoucheva, P. Malaney, S.J. Metallo, R.R. Pathak, A.C. Joerger, Chem. Rev. **114**, 6844 (2014). https://doi.org/10.1021/cr400713r
4. M.K. Tiwari, K.P. Kepp, Alzheimers Dement. **12**, 184 (2016). https://doi.org/10.1016/j.jalz.2015.06.1895
5. G.F. Chen, T.H. Xu, Y. Yan, Y.R. Zhou, Y. Jiang, K. Melcher, H.E. Xu, Acta Pharmacol. Sin. **38**, 1205 (2017). https://doi.org/10.1038/aps.2017.28
6. J.X. Chen, S.S. Yan, J. Alzheimers Dis. **20**, S569 (2010). https://doi.org/10.3233/JAD-2010-100357
7. L. Crews, E. Masliah, Hum. Mol. Genet. **19**, R12 (2010). https://doi.org/10.1093/hmg/ddq160
8. C.L. Masters, G. Simms, N.A. Weinman, G. Multhaupt, B.L. Mcdonald, K. Beyreuthert, Proc. Natl. Acad. Sci. U.S.A. **82**, 4245 (1985). https://doi.org/10.1073/pnas.82.12.4245
9. S. Karantzoulis, J.E. Galvin, Expert Rev. Neurother. **11**, 1579 (2011). https://doi.org/10.1586/ern.11.155
10. J. Busciglio, A. Lorenzo, J. Yeh, B.A. Yankner, Neuron **14**, 879 (1995). https://doi.org/10.1016/0896-6273(95)90232-5
11. S. Tiwari, V. Atluri, A. Kaushik, A. Yndart, M. Nair, Int. J. Nanomed. **14**, 5541 (2019). https://doi.org/10.2147/IJN.S200490
12. World Health Organization, https://www.who.int/news-room/fact-sheets/detail/dementia, accessed October 8, 2024.
13. Alzheimer's Disease International: Dementia statistics, https://www.alzint.org/about/dementia-facts-figures/dementia-statistics/, accessed October 8, 2024.
14. 'Alzheimer's Disease International. 2024. World Alzheimer Report 2024: Global changes in attitudes to dementia.', London, England, 2024.
15. G.E. Fanucci, D.S. Cafiso, Curr. Opin. Struct. Biol. **16**, 644 (2006). https://doi.org/10.1016/j.sbi.2006.08.008
16. S.A. Shelke, S.T. Sigurdsson, Eur. J. Org. Chem. **2012**, 2291 (2012). https://doi.org/10.1002/ejoc.201101434
17. A. Pierro, M. Drescher, Chem. Commun. **59**, 1274 (2023). https://doi.org/10.1039/d2cc05907j
18. G. Jeschke, Emerg. Top. Life Sci. **2**, 9 (2018). https://doi.org/10.1042/ETLS20170143
19. O. Roopnarine, D.D. Thomas, Appl. Magn. Reson. **55**, 79 (2024). https://doi.org/10.1007/s00723-023-01623-x
20. F. Torricella, A. Pierro, E. Mileo, V. Belle, A. Bonucci, Biochimica et Biophysica Acta (BBA)—Proteins and Proteomics **1869**, 140653 (2021). https://doi.org/10.1016/j.bbapap.2021.140653
21. I.D. Sahu, G.A. Lorigan, BioMed Res. Int. **2018**, 1 (2018). https://doi.org/10.1155/2018/3248289

22. T.I. Smirnova, A.I. Smirnov, in *Methods in Enzymology*. ed. by P.Z. Qin, K. Warncke (Academic Press Inc, UK, 2015), p.219
23. G.I. Likhtenshtein, J. Yamauchi, S. Nakatsuji, A.I. Smirnov, R. Tamura, *Nitroxides* (WILEY-VCH Verlag GmbH & Co, Weinheim, 2008)
24. M.-E. Brik, Heterocycles **41**, 2827 (1995). https://doi.org/10.3987/rev-95-469
25. A. Bonucci, M.G. Murrali, L. Banci, R. Pierattelli, Sci. Rep. (2020). https://doi.org/10.1038/s41598-020-77899-x
26. S. Weickert, M. Wawrzyniuk, L.H. John, S.G.D. Rüdiger, M. Drescher, Sci. Adv. (2020). https://doi.org/10.1126/sciadv.aax6999
27. C. Jang, D. Portugal Barron, L. Duo, C. Ma, H. Seabaugh, Z. Guo, ACS Chem. Neurosci. **15**, 86 (2024). https://doi.org/10.1021/acschemneuro.3c00364
28. H.S. Mchaourab, M.A. Lietzow, K. Hideg, W.L. Hubbell, Biochemistry **35**, 7692 (1996). https://doi.org/10.1021/bi960482k
29. C. Altenbach, C.J. López, K. Hideg, W.L. Hubbell, Methods Enzymol. **564**, 59 (2015). https://doi.org/10.1016/bs.mie.2015.08.006
30. J. Stehle, M. Hülsmann, A. Godt, M. Drescher, M. Azarkh, ChemPhysChem **25**, e202300928 (2024). https://doi.org/10.1002/cphc.202300928
31. O. Schiemann, C.A. Heubach, D. Abdullin, K. Ackermann, M. Azarkh, E.G. Bagryanskaya, M. Drescher, B. Endeward, J.H. Freed, L. Galazzo, D. Goldfarb, T. Hett, L.E. Hofer, LFábregas. Ibáñez, E.J. Hustedt, S. Kucher, I. Kuprov, J.E. Lovett, A. Meyer, S. Ruthstein, S. Saxena, S. Stoll, C.R. Timmel, M.D. Valentin, H.S. McHaourab, T.F. Prisner, B.E. Bode, E. Bordignon, M. Bennati, G. Jeschke, J. Am. Chem. Soc. **143**, 17875 (2021). https://doi.org/10.1021/jacs.1c07371
32. A.D. Milov, A.B. Ponomarev, Y.D. Tsvetkov, Chem. Phys. Lett. **110**, 67 (1984). https://doi.org/10.1016/0009-2614(84)80148-7
33. A.D. Milov, A.G. Maryasov, Y.D. Tsvetkov, Appl. Magn. Reson. **15**, 107 (1998). https://doi.org/10.1007/BF03161886
34. I. Krstić, R. Hänsel, O. Romainczyk, J.W. Engels, V. Dötsch, T.F. Prisner, Angew. Chem. Int. Ed. **50**, 5070 (2011). https://doi.org/10.1002/anie.201100886
35. R. Igarashi, T. Sakai, H. Hara, T. Tenno, T. Tanaka, H. Tochio, M. Shirakawa, J. Am. Chem. Soc. **132**, 8228 (2010). https://doi.org/10.1021/ja906104e
36. L.V. Kulik, S.A. Dzuba, I.A. Grigoryev, Y.D. Tsvetkov, Chem. Phys. Lett. **343**, 315 (2001). https://doi.org/10.1016/S0009-2614(01)00721-7
37. K. Ackermann, C.A. Heubach, O. Schiemann, B.E. Bode, J. Phys. Chem. Lett. **15**, 1455 (2024). https://doi.org/10.1021/acs.jpclett.3c03311
38. C.S. Klug, J.B. Feix, Methods Cell Biol. **84**, 617 (2008). https://doi.org/10.1016/S0091-679X(07)84020-9
39. K. Ackermann, A. Chapman, B.E. Bode, Molecules **26**, 7534 (2021). https://doi.org/10.3390/molecules26247534
40. J.J. Falkel, A.F. Dernburg, D.A. Sternberg, N. Zalkin, D.L. Milligan, D.E. Koshland, J. Biol. Chem. **263**, 14850 (1988). https://doi.org/10.1016/S0021-9258(18)68117-7
41. P.L. Tsai, S.F. Chen, S.Y. Huang, Rev. Anal. Chem. **32**, 257 (2013). https://doi.org/10.1515/revac-2013-0011
42. M.J. Lawless, A. Shimshi, T.F. Cunningham, M.N. Kinde, P. Tang, S. Saxena, Chem. Phys. Chem. **18**, 1653 (2017). https://doi.org/10.1002/cphc.201700115
43. M. Martinho, D. Allegro, I. Huvent, C. Chabaud, E. Etienne, H. Kovacic, B. Guigliarelli, V. Peyrot, I. Landrieu, V. Belle, P. Barbier, Sci. Rep. **8**, 13846 (2018). https://doi.org/10.1038/s41598-018-32096-9
44. M. Azarkh, O. Okle, P. Eyring, D.R. Dietrich, M. Drescher, J. Magn. Reson. **212**, 450 (2011). https://doi.org/10.1016/j.jmr.2011.07.014
45. Z. Hasanbasri, K. Singewald, T.D. Gluth, B. Driesschaert, S. Saxena, J. Phys. Chem. B **125**, 5265 (2021). https://doi.org/10.1021/acs.jpcb.1c02371
46. M.R. Fleissner, E.M. Brustad, T. Kálai, C. Altenbach, D. Cascio, F.B. Peters, K. Lmá Hideg, S. Peuker, P.G. Schultz, W.L. Hubbell, Biophys. Comput. Biol. (2009). https://doi.org/10.1073/pnas.0912009106
47. M.J. Schmidt, A. Fedoseev, D. Bücker, J. Borbas, C. Peter, M. Drescher, D. Summerer, ACS Chem. Biol. **10**, 2764 (2015). https://doi.org/10.1021/acschembio.5b00512
48. S. Kucher, S. Korneev, S. Tyagi, R. Apfelbaum, D. Grohmann, E.A. Lemke, J.P. Klare, H.J. Steinhoff, D. Klose, J. Magn. Reson. **275**, 38 (2017). https://doi.org/10.1016/j.jmr.2016.12.001

49. C.C. Liu, P.G. Schultz, Annu. Rev. Biochem. **79**, 413 (2010). https://doi.org/10.1146/annurev.biochem.052308.105824
50. R.B. Merrifield, J. Am. Chem. Soc. **85**, 2149 (1963). https://doi.org/10.1021/ja00897a025
51. R.B. Merrifield, J.M. Stewart, Nature **207**, 522 (1965). https://doi.org/10.1038/207522a0
52. S.M. Marino, V.N. Gladyshev, J. Mol. Biol. **404**, 902 (2010). https://doi.org/10.1016/j.jmb.2010.09.027
53. N.M. Giles, A.B. Watts, G.I. Giles, F.H. Fry, J.A. Littlechild, C. Jacob, Chem. Biol. **10**, 677 (2003). https://doi.org/10.1016/S1074-5521(03)00174-1
54. P. Widder, F. Berner, D. Summerer, M. Drescher, ACS Chem. Biol. **14**, 839 (2019). https://doi.org/10.1021/acschembio.8b01111
55. A.K. Schütz, T. Vagt, M. Huber, O.Y. Ovchinnikova, R. Cadalbert, J. Wall, P. Güntert, A. Bcöckmann, R. Glockshuber, B.H. Meier, Angewandte Chemie—International Edition **54**, 331 (2015). https://doi.org/10.1002/anie.201408598
56. J.X. Lu, W. Qiang, W.M. Yau, C.D. Schwieters, S.C. Meredith, R. Tycko, Cell **154**, 1257 (2013). https://doi.org/10.1016/j.cell.2013.08.035
57. A. Rostagno, J.L. Holton, T. Lashley, T. Revesz, J. Ghiso, Cell. Mol. Life Sci. **67**, 581 (2010). https://doi.org/10.1007/s00018-009-0182-4
58. J. Kardos, M.P. Nyiri, É. Moussong, F. Wien, T. Molnár, N. Murvai, V. Tóth, H. Vadászi, J. Kun, F. Jamme, A. Micsonai, Protein Sci. **34**, e70066 (2025). https://doi.org/10.1002/pro.70066
59. I. Sepkhanova, M. Drescher, N.J. Meeuwenoord, R.W.A.L. Limpens, R.I. Koning, D.V. Filippov, M. Huber, Appl. Magn. Reson. **36**, 209 (2009). https://doi.org/10.1007/s00723-009-0019-1
60. M. Robotta, Ph.D. Thesis Universität Konstanz, 2014.
61. S. Stoll, A. Schweiger, J. Magn. Reson. **178**, 42 (2006). https://doi.org/10.1016/j.jmr.2005.08.013